B. Casal (on behalf of the CDF Collaboration)

Instituto de Física de Cantabria (CSIC-Univ. Cantabria), Avda. de los Castros s/n, 39005 Santander, Spain

We present recent CDF results based on approximately 1 fb^{-1} of $p\bar{p}$ collisions at $\sqrt{s} = 1.96$ TeV delivered at Fermilab Tevatron. Results shown include the observation of the B_s oscillation frequency, the first observation of bottom baryon $\Sigma_b^{(*)\pm}$ states, updates on B hadrons lifetimes, and searches for rare decays in the $b \to s\mu^+\mu^-$ transition and in charmless two-body B decays.

1. Introduction

The Tevatron collider at Fermilab, operating at $\sqrt{s} = 1.96$ TeV, has a huge $b\bar{b}$ production cross section which is several orders of magnitude larger than the production rate at e^+e^- colliders running on the $\Upsilon(4S)$ resonance. In addition, on the $\Upsilon(4S)$ only B^+ and B_d^0 are produced, while higher mass b-hadrons such as B_s^0, B_c, b-baryons, B^*, and p-wave B mesons are currently produced only at Tevatron. In order to exploit the possibility to study those variety of heavy b-hadrons in a busy hadronic environment, dedicated detector systems, trigger and reconstruction are crucial.

In the following subsections we briefly describe the Tevatron collider, the CDF II detector, and the trigger strategies used at CDF for heavy flavor physics. Then, in the following sections we discuss the most recent and interesting heavy flavor results at CDF.

1.1. The Tevatron Collider

Tevatron is a superconducting proton-synchrotron at the final stage of the Fermilab accelerator complex. In Run II (mid-2001–present), it accelerates 36 bunches of protons against 36 bunches of anti-protons producing one crossing every 396 ns at $\sqrt{s} = 1.96$ TeV. The luminous region of the Tevatron beam has an RMS of ~ 30 cm along the beamline (z-direction) with a transverse beamwidth of about 30 μm.

The instantaneous luminosity has been rising steadily during Run II up to the world record peak of 2.92×10^{32} cm^{-2}s^{-1}, and regularly exceeds 2×10^{32} cm^{-2}s^{-1}. The machine typically delivers data corresponding to an integrated luminosity of > 30 pb^{-1} per week, which is recorded with an average data-taking efficiency of about 85% at CDF. The increase in accelerator performance throughout Run II can be seen by the delivered luminosity per calendar year, as shown in Fig. 1. As of May 2007, the total integrated luminosity delivered by the Tevatron to CDF is ~ 2.7 fb^{-1} with about 2.2 fb^{-1} recorded to tape by the CDF experiment. However, most results presented here are based on about 1 fb^{-1} of data.

Around 8 fb^{-1} are expected to be delivered until the shutdown of the Tevatron end in 2009.
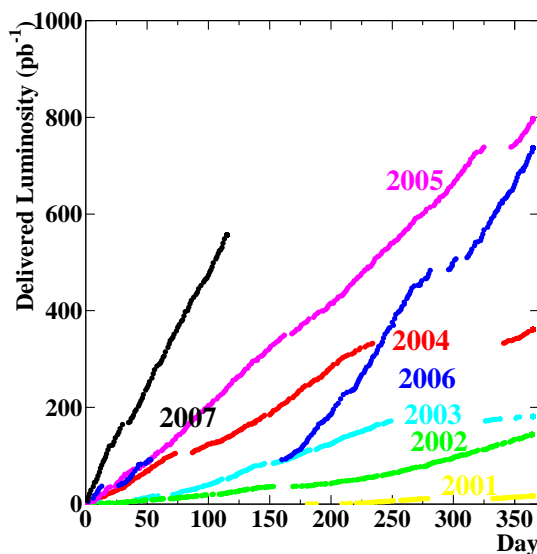

Figure 1: Tevatron delivered luminosity per calendar year up to May 2007.

1.2. The CDF II Detector

The CDF II detector is a 5000 t, multipurpose, solenoidal magnetic-spectrometer surrounded by 4π calorimeters and muon detectors, it is axially and azimuthally symmetric around the interaction point. Its excellent tracking performance, good muon coverage, and particle identification (PID) capabilities allow a broad flavor-physics program. We briefly outline the sub-detectors pertinent to the analyses described here, additional details can be found elsewhere [1].

The CDF II tracking system consist of an inner silicon system surrounded by a cylindrical gas-wire drift chamber, both immersed in a 1.4 T solenoidal magnetic field with 135 cm total lever arm. Six (central region, $|\eta| < 1$) to seven (forward, $1 < |\eta| < 2$) double-sided silicon layers, plus one single-sided layer, extend radially from 1.6 to 22 cm (28 cm) from the beam line

in the central (forward) region, fully covering the luminous region. The chamber provides 96 (48 axial and 48 stereo) samplings of charged-particle paths between 40 and 137 cm from the beam, and within $|\eta| < 1$. The long lever arm of the tracker provides a superb mass-resolution with $\sigma(p_T)/p_T^2 \sim 0.1\%$ GeV^{-1}. In addition, silicon measurements close to the beam allow precise reconstruction of decay vertexes, with typical resolution of 35 μm in the transverse plane –shown in Fig. 2, which includes a contribution of 32 μm from the width of the $p\bar{p}$ interaction region– and 70 μm along the beam direction.

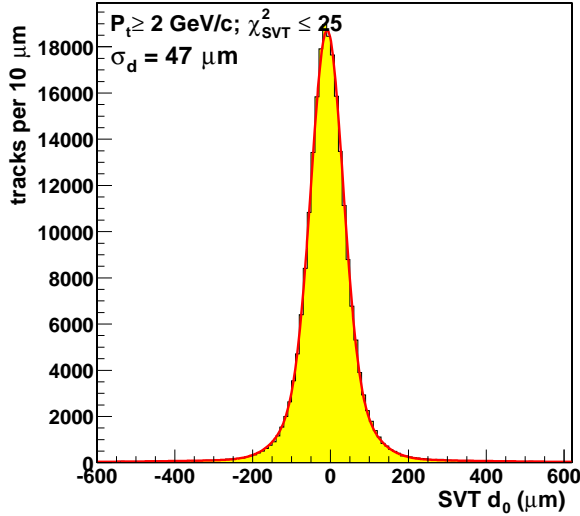Figure 2: Impact parameter resolution provided by the silicon micro-vertex detector. The resolution is 47 μm, while the typical heavy flavor trigger requires tracks with impact parameter grater than 120 μm.

Four layers of planar drift chambers detect muon candidates with $p_T > 1.4$ GeV/c in the $|\eta| < 0.6$ region, while conical sections of drift tubes extend the coverage to $0.6 < |\eta| < 1.0$ for muon candidates with $p_T > 2.0$ GeV/c.

Low momentum PID is obtained with a scintillator based Time-of-Flight (TOF) detector with about 110 ps resolution, that provides a separation between kaons and pions greater than 2σ for charged particles with $p < 1.5$ GeV/c, see Fig. 3(left). The information of specific energy loss from the drift chamber (dE/dx) complements the PID with a nearly constant 1.4σ K/π separation for higher momentum charged particles ($pT > 2.0$ GeV/c), see Fig. 3(right).

1.3. Trigger Strategies

CDF exploits its unique ability to trigger events with charged particles originated in vertexes displaced from the primary $p\bar{p}$ vertex (displaced tracks) [2]. Displaced tracks are identified by measuring with 35 μm intrinsic resolution their impact parameter (see

Fig. 2), which is the minimum distance between the particle direction and the primary $p\bar{p}$ vertex in the plane transverse to the beam. Such a high accuracy can be reached only using online the silicon information, a challenging task that requires to read-out 212,000 silicon channels and to complete hit-clustering and pattern recognition within the trigger latency. In a highly parallelized architecture, fast pattern matching and linearized track fitting allow reconstruction of 2D-tracks in the plane transverse to the beam with offline quality by combining drift chamber and silicon information, within a typical latency of 25 μs per event. Using the above device, CDF implemented a trigger selection that requires only two displaced tracks in the event, to collect pure samples of exclusive non-leptonic b-decays for the first time in a hadron collider. However, an impact-parameter based selection biases the decay-length distributions, and therefore a trigger efficiency dependence –that models the acceptance as a function of proper decay time– must be taken into account for time dependent measurements.

Besides the trigger on displaced tracks, past experience from Run I suggests that triggering on final states containing single leptons or dileptons is a successful strategy to select samples of b-hadron decays, since semileptonic ($B \to \ell\nu_\ell X$) and charmonium ($B \to J/\psi[\ell^+\ell^-]X$) decays represent about 20% of b-meson widths and have relatively clean experimental signatures. Such a 'conventional' approach was adapted to the upgraded detector: identification of muon down to low momenta allows for efficient dimuon triggers in which we select charmonium or rare decays and then we fully reconstruct several decay modes. On the other hand, semileptonic triggers require a displaced track in addition to the muon (or electron), providing cleaner samples.

2. Measurement of $B_s^0 - \overline{B}_s^0$ Oscillation Frequency

The precise determination of the $B_s^0 - \overline{B}_s^0$ oscillation frequency Δm_s from a time-dependent analysis of the $B_s^0 - \overline{B}_s^0$ system has been one of the most important goals for heavy flavor physics at the Tevatron. This frequency can be used to strongly improve the knowledge of the Cabbibo-Kobayashi-Maskawa (CKM) matrix, and to constraint contributions from New Physics.

The probability $\mathcal{P}$ for a B_s meson produced at time $t = 0$ to decay as a B_s ($\overline{B}_s$) at proper time $t > 0$ is, neglecting effects from CP violation as well as possible lifetime difference between the heavy and light B_s^0 mass eigenstates, given by

$$\mathcal{P}_\pm(t) = \frac{\Gamma_s}{2}e^{-\Gamma_s t}\left[1 \pm \cos\left(\Delta m_s t\right)\right], \qquad (1)$$
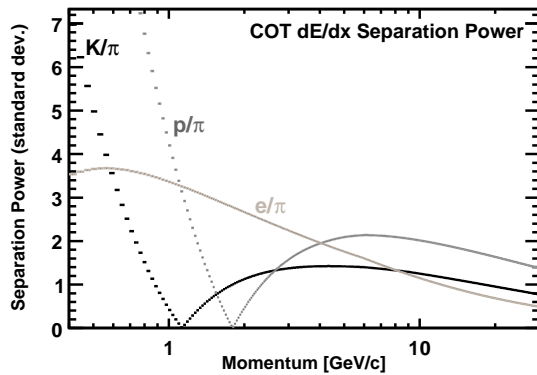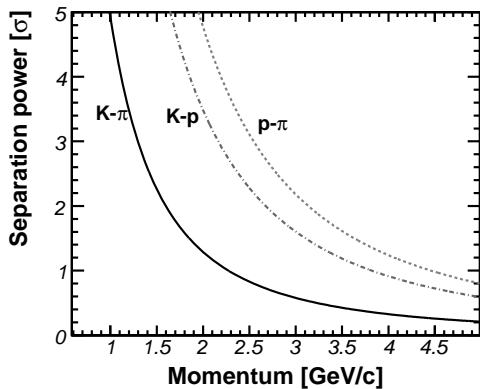
Figure 3: Particle identification separation power in units of standard deviations provided by the TOF detector (left) and the drift chamber dE/dx (right).

where the subscript "+" ("-") indicates that the meson decays as B_s ($\overline{B}_s$). Oscillations have been observed and well established in the B_d system. The mass difference Δm_d is measured to be $\Delta m_d = 0.505\pm 0.005$ ps^{-1} [3].

In the $B_s^0 - \overline{B}_s^0$ system oscillation have also been established but till winter 2006 all attempts to measure Δm_s have only yielded a combined lower limit on the mixing frequency of $\Delta m_s > 14.5$ ps^{-1} at 95% confidence level (C.L.). Indirect fits constraint Δm_s to be below 24 ps^{-1} at 95% C.L. within the standard model. In the 2006 spring the D0 experiment presented the first double sided 90% C.L. limit [4] and CDF shortly afterwards presented the first precision measurement on Δm_s, with a significance of the signal of about 3σ at that time [5]. Just a few months later the CDF collaboration updated their result using the same data, but improved analysis techniques and were able to announce the observation of the $B_s^0 - \overline{B}_s^0$ mixing frequency [6].

The canonical B mixing analysis proceeds as follows. The b flavor (b or $\bar{b}$ of the B meson at the time of decay) is determined from the charges of the reconstructed decay products in the final state. The proper time at which the decay occurred is determined from the transverse displacement of the B_s decay vertex with respect to the primary vertex, and the B_s transverse momentum with respect to the proton beam. Finally the production b flavor must be known in order to classify the B meson as being mixed (production and decay b flavor are different) or unmixed (production and decay b flavor are equal) at the time of its decay.

The significance $\mathcal{S}$ of a mixing signal is given by:

$$\mathcal{S} \sim \sqrt{\frac{\epsilon D^2}{2}} \times \frac{S}{\sqrt{S+B}} \times \exp\left(-\frac{\Delta m_s^2 \sigma_{ct}^2}{2}\right), \quad (2)$$

where S and B are the signal and background event yields, respectively. $\epsilon \mathcal{D}^2$ is the figure of merit for the flavor tagging, where ϵ is the efficiency to tag a given B_s decay candidate, and $\mathcal{D} = 1 - P_w$ is the so-called dilution, a damping term which is related to the imperfect tagging, being P_w the probability of a wrong tag. σ_{ct} is the proper decay time resolution, which is crucial for this analysis especially at large Δm_s values.

We will in the following sections discuss those various ingredients to the mixing analysis –focusing in the improvements with respect to the analysis [5] presented in last year FPCP conference– and then present the result.

2.1. Signal Yields

Several improvements with respect to the analysis in Ref [5] lead to an increased B_s signal yield. The decay sequences used are the hadronic channels $\bar{B}_s^0 \to D_s^+ \pi^-$, $D_s^+ \pi^- \pi^+ \pi^-$ and the semileptonic channels $\bar{B}_s^0 \to D_s^{+(*)} \ell^- \bar{\nu}_\ell$, $\ell = e$ or μ, where $D_s^+ \to \phi\pi^+$, $K^*(892)^0 K^+$, and $\pi^+\pi^-\pi^+$, and $\phi \to K^+K^-$, $K^{*0} \to K^-\pi^+$.

Particle identification techniques provided by the TOF and dE/dx information are used to find kaons from D_s meson decays, allowing us to relax kinematic selection requirements on the D_s decay products. This results in increased efficiency for reconstructing the D_s meson while maintaining excellent signal to background ratio.

In the semileptonic channel, the main gain is in the $D_s^+ \ell^-$, $D_s^+ \to \bar{K}^*(892)^0 K^+$ sequence, where the signal is increased by a factor of 2.2 using the particle identification techniques. An additional gain in signal by a factor of 1.3 with respect to our previous analysis comes from adding data selected with different trigger requirements. In total, the signal of 37,000 semileptonic B_s decays in [5] is increased to 61,500, and the signal to background improves by a factor of two in the sequences with kaons in the final state.

In the hadronic channels, we employ an artificial neural network (ANN) to improve candidate selection resulting in larger signal yields at similar or smaller background levels. The ANN selection makes it possible to use the additional decay sequence $\bar{B}_s^0 \to D_s^+ \pi^- \pi^+ \pi^-$, with $D_s^+ \to \pi^+ \pi^- \pi^+$, as well. The neural network is trained using simulated signals events generated with Monte Carlo methods. For combinatorial background, we use sideband regions in the upper-mass distribution of the B_s candidates from data. We add significant statistics using the partially reconstructed hadronic signal between 5.0 and 5.3 GeV/c^2 from $\bar{B}_s^0 \to D_s^{*+} \pi^-$, $D_s^{*+} \to D_s^+ \gamma/\pi^0$ in which a photon or a π^0 from the D_s^{*+} is missing and $\bar{B}_s^0 \to D_s^+ \rho^-$, $\rho^- \to \pi^- \pi^0$ in which a π^0 is missing. The mass distribution for the highest statistical mode, $\bar{B}_s^0 \to D_s^+ (\phi\pi^+)\pi^-$, as well as for the partially reconstructed modes is shown in Fig. 4. Table I summarizes the signal yields.
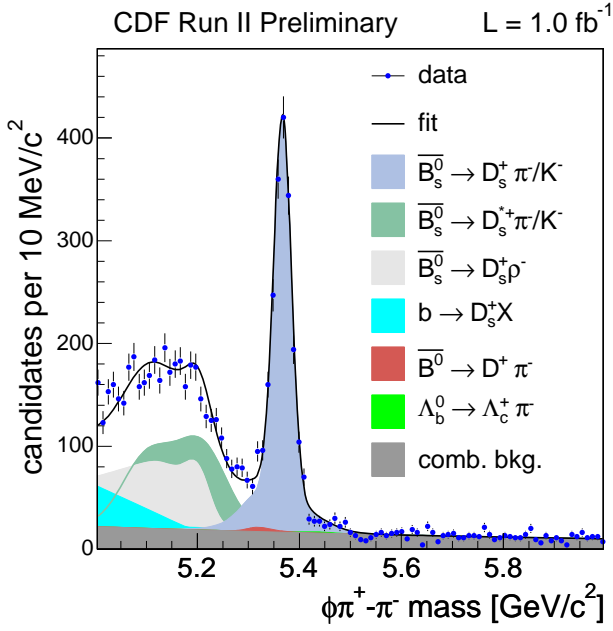
Table I Signal yields (S) and signal to background ratio (S/B) in the hadronic decay sequences. The gain refers to the percentage increase in $S/\sqrt{S+B}$.

Decay Sequence	Signal	S/B	gain [%]
$\bar{B}_s^0 \to D_s^+ [\phi\pi^+]\pi^-$	1900	11.3	13
Partially reconstructed	3300	3.4	new
$\bar{B}_s^0 \to D_s^+ [K^{*0}K^+]\pi^-$	1400	2.0	35
$\bar{B}_s^0 \to D_s^+ [(3\pi)^+]\pi^-$	700	2.1	22
$\bar{B}_s^0 \to D_s^+ [\phi\pi^+](3\pi)^-$	700	2.7	92
$\bar{B}_s^0 \to D_s^+ [K^{*0}K^+](3\pi)^-$	600	1.1	110
$\bar{B}_s^0 \to D_s^+ [(3\pi)^+](3\pi)^-$	200	2.6	new

Figure 4: Invariant mass distribution of $\bar{B}_s^0 \to D_s^+(\phi\pi^+)\pi^-$ candidates.

With all these improvements, the statistical size of our data sample is increased by a factor of 2.5.

2.2. Decay Length Resolution

One of the critical input to the analysis is the proper decay time resolution. It is the limiting factor of the sensitivity of the signal at large Δm_s values. For setting a limit a too optimistic proper decay time resolution estimate could potentially lead to the exclusion of Δm_s regions we are actually not sensitive to. Therefore σ_{ct} has been measured directly on data. CDF

exploits prompt D decays plus tracks from the primary vertex to mimic all B decay topologies studied in this analysis. On an event-by-event basis, the decay time resolution is predicted, taking into account dependences on several variables, such as isolation, vertex χ^2, etc. The mean σ_{ct} for hadronic events at CDF is 26 μm and for semileptonic events about 45 μm. This excellent decay length resolution is reached at CDF thanks to the innermost silicon layer at a distance of about 1.2 cm from the collision point.

2.3. Flavor Tagging

While the flavor of the B_s candidate at decay time is unambiguously defined by the charges of its daughter tracks, the flavor at production can be inferred, with a certain degree of uncertainty, by flavor tagging algorithms. Two type of flavor tags can be applied: opposite-side and same-side flavor tags. Opposite-side tags infer the production flavor of the B_s from the decay products of the B hadron produced from the other b quark in the event. Lepton tagging algorithms are based on semileptonic b decays into an electron or muon ($b \to \ell^- X$). The charge of the lepton is thus correlated to the charge of the decaying B hadron. Jet charge tagging algorithms use the fact that the charge of a b jet is correlated to the charge of the b quark. Kaon tagging are based on the CKM favored quark level decay sequence ($b \to b \to s$). The charge of the kaon from opposite-side B decays is correlated to the b flavor. CDF combines these three tagging techniques using a Neural Network approach. The performance of the opposite-side flavor tagging algorithm is measured in kinematically similar B_d and B^+ semileptonic samples. The Δm_d value is found to be $\Delta m_d = 0.509 \pm 0.010$ (stat.) ± 0.016 (syst.) ps^{-1}, which agrees well with the world average [3].

CDF yields a combined opposite-side tagging performance of $\epsilon\mathcal{D}^2 = 1.8\%$, which is an improvement of 20% with respect to the previous CDF analysis [5].

Same-side flavor tags are based on the charges of associated particles produced in the fragmentation of

the b quark that produces the reconstructed B_s. Contrary to the opposite-side tagging algorithms, the performance of this tagging algorithm can not be calibrated on B_d and B^+ data, but we have to rely on Monte Carlo samples until a significant B_s mixing signal has been established. CDF uses Neural Network techniques to combine kaon particle identification variables from dE/dx measurements in the drift-chamber and time-of-flight measurements with kinematic quantities of the kaon candidate into a single tagging variable. Tracks close in phase space to the B_s candidate are considered as same-side kaon tag candidates, and the track with the largest value of the tagging variable is selected as the tagging track. We predict the dilution of the same-side tag using simulated data samples generated with the PYTHIA [7] Monte Carlo program. The predicted fractional gain in $\epsilon\mathcal{D}^2$ from using the Neural Network is 10%. Control samples of B^+ and B_d are used to validate the predictions of the simulation. The tagging power of this flavor tag is $\epsilon\mathcal{D}^2 = 3.7(4.8)\%$ for the hadronic (semileptonic) decay sample. If both a same-side tag and an opposite-side tag are present, we combine the information from both tags assuming they are independent.

2.4. Fit and Results

An unbinned maximum likelihood fit is used to search for $B_s^0 - \overline{B}_s^0$ oscillations. The likelihood combines mass, proper decay time, proper decay time resolution and flavor tagging information for each candidate. Separate probability density functions are used to describe signal and each type of background. The amplitude scan method [8] was used to search for oscillations. The likelihood term describing the proper decay time of tagged B_s meson candidates in Eq. 1 is modified by introducing the amplitude $\mathcal{A}$:

$$\mathcal{L} \sim 1 \pm \mathcal{A}\mathcal{D}\cos(\Delta mt). \quad (3)$$

Then, a scan in Δm is performed by fitting $\mathcal{A}$ for fixed values of Δm. The dilution $\mathcal{D}$ is fixed to the value obtained by the calibration process. This procedure corresponds to a Fourier transformation of the proper time space into the frequency space. In the case of infinite statistics and perfect resolution, it is expected to find $\mathcal{A} = 1$ for the vicinity of true value of Δm and $\mathcal{A} = 0$ otherwise. In practice, the procedure consists in recording $(\mathcal{A}, \sigma_\mathcal{A})$ for each Δm hypothesis. A particular value of Δm is excluded at 95% C.L. if $\mathcal{A} + 1.645\sigma_\mathcal{A} < 1$ holds. The sensitivity of a mixing analysis is defined as the lowest Δm value for which $1.645\sigma_\mathcal{A} = 1$.

The combined amplitude scans for the analysis of the hadronic and semileptonic B_s candidates and the combined result are shown separately in Fig. 5. The combined sensitivity is 31.3 ps^{-1}. The value of the

amplitude is consistent with unity around $\Delta m_s = 17.75$ ps^{-1}, where $\mathcal{A} = 1.21 \pm 0.20$. Elsewhere, the amplitude is always consistent with zero (Fig. 5). The minimum likelihood ratio Λ is at $\Delta m_s = 17.77$ ps^{-1} and has a value of -17.26. The significance of the signal is given by the probability that randomly tagged data would produce a value of Λ lower than -17.26 at any value of Δm_s. Only 28 out of 350 million generated toy experiments yielded a Λ value lower than that. This results in a p-value of 8×10^{-8} which corresponds to a 5.4σ signal. The fit for Δm_s, with $\mathcal{A}$ fixed to unity, finds

$$\Delta m_s = 17.77 \pm 0.10(\text{stat.}) \pm 0.07(\text{syst.}) \text{ ps}^{-1}. \quad (4)$$

The dominant contributions to the systematic uncertainties comes from uncertainties on the absolute scale of the decay-time measurement.

Combining the measured Δm_s value with the well known Δm_d value CDF derive the following ratio of the CKM matrix elements:

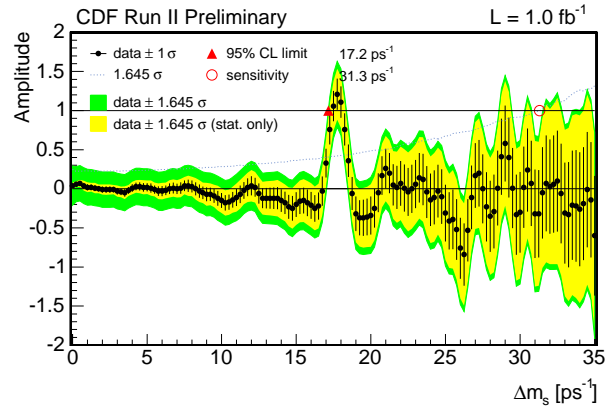$$\left|\frac{V_{td}}{V_{ts}}\right| = 0.2060 \pm 0.0007(\text{exp.})^{+0.0080}_{-0.0060}(\text{theor.}). \quad (5)$$

Figure 5: Amplitude scan of the hadronic and semileptonic decay modes combined.

3. Observation of New Σ_b Baryon

Until recently only one bottom baryon, the Λ_b^0, has been directly observed. At present the CDF collaboration has accumulated the world's largest data sample of bottom baryons, due to a combination of two factors: the CDF displaced track trigger, and the ~ 1 fb^{-1} of integrated luminosity delivered by the Tevatron. Using a sample of fully reconstructed $\Lambda_b^0 \rightarrow \Lambda_c^+\pi^-$ candidates collected with the displaced track trigger, CDF searched for the decay $\Sigma_b^{(*)\pm} \rightarrow \Lambda_b^0\pi^\pm$.

CDF reconstructs the decay chain $\Lambda_b^0 \rightarrow \Lambda_c^+\pi^-$, $\Lambda_c^+ \rightarrow pK^-\pi^+$, reaching a Λ_b^0 yield of approximately 2800 candidates in the signal region $m(\Lambda_b^0) \in$

[5.565, 5.670] GeV/c². The Λ_b^0 mass plot is shown in Fig. 6.

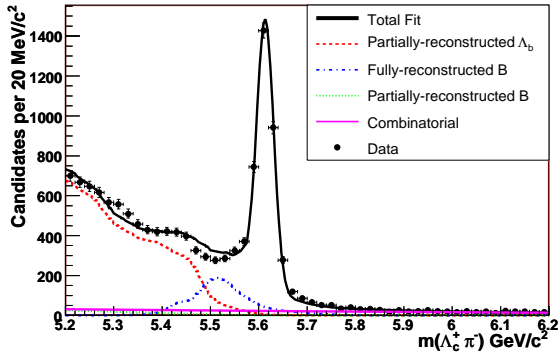Figure 6: Fit to the invariant mass of $\Lambda_b^0 \to \Lambda_c^+ \pi^-$ candidates. The discrepancies between the fit and data below the Λ_b^0 signal region are due to incomplete knowledge of the branching ratios of the decays in this region and are included in the $\Sigma_b^{(*)}$ background model systematics.

To separate out the resolution on the mass of each Λ_b^0 candidate, CDF searches for narrow resonances in the mass difference distribution of $Q = m(\Lambda_b^0 \pi) - m(\Lambda_b^0) - m_\pi$. Unless explicitly stated, Σ_b refers to both the $J = \frac{1}{2}(\Sigma_b^\pm)$ and $J = \frac{3}{2}(\Sigma_b^{*\pm})$ states. There is no transverse momentum cut applied to the pion from the Σ_b decay, since these tracks are expected to be very soft. In order to perform an unbiased search, the cuts for the Σ_b reconstruction are optimized first with the Σ_b signal region blinded. From theoretical predictions the Σ_b signal region is chosen as $30 < Q < 100$ MeV/c², while the upper and lower sideband regions of $0 < Q < 30$ MeV/c² and $100 < Q < 500$ MeV/c² represent the Σ_b background. The signal for the optimization is taken from a PYTHIA Monte Carlo Σ_b sample, with the decays $\Sigma_b \to \Lambda_b^0 \pi$, $\Lambda_b^0 \to \Lambda_c^+ \pi^-$, $\Lambda_c^+ \to p K^- \pi^+$ forced.

The backgrounds under the Λ_b^0 signal region in the Λ_b^0 mass distribution will also be present in the Σ_b Q-distribution. The primary sources of background are Λ_b^0 hadronization and underlying event, hadronization and underlying event of other B meson reflections and combinatorial background underneath the Λ_b^0 peak. The percentage of each background component in the Λ_b^0 signal region is derived from the Λ_b^0 mass fit, and is determined as 86% Λ_b^0 signal, 9% backgrounds and 5% combinatorial background. Other backgrounds (e.g. from 5-track decays where one track is taken as the π_{Σ_b} candidate) are negligible, as confirmed in inclusive single-b-hadron Monte Carlo samples.

Upon unblinding the Q signal region, there is an excess observed in data over predicted backgrounds. CDF performs a simultaneous unbinned likelihood fit to "same charge" and "opposite charge" data. To the already described background components, four peaks are added, one for each of the expected Σ_b

states. Each peak is described by a non-relativistic Breit-Wigner convoluted with two Gaussian resolution functions. The detector resolution has a dominant narrow core and a small broader shape describing the tails where the PDF for each peak takes both into account. Due to low statistics, CDF constrains $m(\Sigma_b^{*+}) - m(\Sigma_b^+)$ and $m(\Sigma_b^{*-}) - m(\Sigma_b^-)$ to be the same. The results of the fit are displayed in Fig. 7.
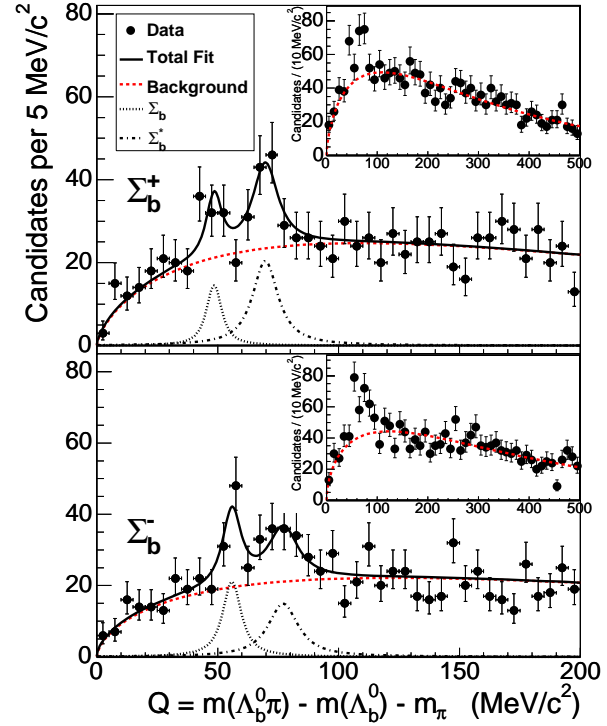

Figure 7: Simultaneous fit to the Σ_b states. Top plots cotains $\Sigma_b^{(*)+}$ states, while the bottom plots contains $\Sigma_b^{(*)-}$ states. The insets show the expected background plotted on the data, while the signal fit is shown on a reduced range of Q.

All systematic uncertainties on the mass difference measurements are small compared to their statistical errors.

To summarize, the lowest lying charged $\Lambda_b^0 \pi$ resonant states are observed in 1 fb^{-1} of data collected by the CDF detector. These are consistent with the lowest lying charged $\Sigma_b^{(*)\pm}$ baryons. Using the best CDF mass measurement for the Λ_b^0 mass, which is $m(\Lambda_b^0) = 5619.7 \pm 1.2(\text{stat.}) \pm 1.2(\text{syst.})$ MeV/c², the absolute mass values are measured to be:

$$m(\Sigma_b^-) = 5815.2 \pm 1.0(\text{stat.}) \pm 1.7(\text{syst.}) \text{ MeV}$$
$$m(\Sigma_b^+) = 5807.8^{+2.0}_{-2.2}(\text{stat.}) \pm 1.7(\text{syst.}) \text{ MeV}$$
$$m(\Sigma_b^{*-}) = 5836.4 \pm 2.0(\text{stat.})^{+1.8}_{-1.7}(\text{syst.}) \text{ MeV}$$
$$m(\Sigma_b^{*+}) = 5829.0^{+1.6}_{-1.8}(\text{stat.})^{+1.7}_{-1.7}(\text{syst.}) \text{ MeV}$$

4. Lifetimes Measurements in J/ψ Decays

In a simple quark spectator model, the lifetime of a B hadron is governed by the decay of the b-quark, and the lifetimes of all B hadrons are expected to be the same. However, because of significant non-spectator effects, the B hadron lifetimes follow a hierarchy: $\tau(B^+) \geq \tau(B^0) \sim \tau(B_s^0) > \tau(\Lambda_b^0) \gg \tau(B_c^+)$. This hierarchy is predicted by the Heavy Quark Expansion (HQE) technique [9], which expresses decay widths of heavy hadrons as an expansion in inverse powers of the heavy quark mass (i.e. $1/m_b$).

CDF presents an updated measurement of exclusive B lifetimes in the modes $B^+ \rightarrow J/\psi K^+$, $B^0 \rightarrow J/\psi K^{*0}$, $B^0 \rightarrow J/\psi K_s^0$, $B_s \rightarrow J/\psi \phi$ and $\Lambda_b \rightarrow J/\psi \Lambda$, based on 1.0 fb^{-1} of integrated luminosity collected with the di-muon trigger.

Signal yields for all decay channels and measured lifetimes for B^+, B^0, B_s and Λ_b are summarized in Table II and compared with other experiments and PDG2006 average [10] in Fig. 8.

Table II Signal yields for all the channels and measured lifetimes. First uncertainty is statistical and the second is systematic.

Decay Channel	Signal Yield	Lifetime [ps]
$B^+ \rightarrow J/\psi K^+$	12,900	$1.630 \pm 0.016 \pm 0.011$
$B^0 \rightarrow J/\psi K^{*0}$	4,800	$1.551 \pm 0.019 \pm 0.011$
$B^0 \rightarrow J/\psi K_s^0$	3,600	
$B_s \rightarrow J/\psi \phi$	1,100	$1.494 \pm 0.054 \pm 0.009$
$\Lambda_b \rightarrow J/\psi \Lambda$	530	$1.580 \pm 0.077 \pm 0.012$

Results of the B^+ and B^0 mesons lifetimes are in good agreement with the world average, with uncertainties that are comparable to individual uncertainties from B factories results. The measured lifetime for the B_s meson also agrees well with the world average, and its uncertainty is more precise than the global uncertainty from the world average.

The Λ_b lifetime result is the most precise measurement to date. It is consistent with most of individual results from other experiments, although it is $\sim 3\sigma$ above the world average. An independent recent result from CDF has also shown a similar trend above the world average.

5. $B \rightarrow \mu^+ \mu^- h$ Searches

The decay of a b quark into an s quark and two muons requires a flavor-changing neutral current (FCNC) process which is strongly suppressed in the standard model. New physics models allow for significant deviations from the standard model prediction.

While the $b \rightarrow s\gamma$ branching ratio has been accurately measured [10] and agrees with the theory predictions, the $b \rightarrow s\mu^+\mu^-$ transition allows the study of FCNC in more detail through additional observables, such as the dimuon invariant mass, and the forward-backward asymmetry of the strange quark in the dimuon system.

The rare decays $B^+ \rightarrow \mu^+\mu^- K^+$ and $B^0 \rightarrow \mu^+\mu^- K^{*0}$ have been observed at the B factories [11, 12]. However, searches for the analogous $B_s \rightarrow \mu^+\mu^-\phi$ decay, with a predicted branching ratio of 1.6×10^{-6} [13], have not revealed a significant signal.

CDF search in 924 pb^{-1} of data for the rare decay modes $B^+ \rightarrow \mu^+\mu^- K^+$, $B^0 \rightarrow \mu^+\mu^- K^{*0}$ and $B_s \rightarrow \mu^+\mu^-\phi$. The K^* is reconstructed in the mode $K^* \rightarrow K^+\pi^-$, and the ϕ is reconstructed as $\phi \rightarrow K^+K^-$.

The offline analysis begins by searching for a pair of oppositely charged muon tracks. The two muon tracks are combined with a third charged track from a $B^+ \rightarrow \mu^+\mu^- K^+$ candidate, or another pair of oppositely charged tracks from a $B^0 \rightarrow \mu^+\mu^- K^{*0}$ or $B_s \rightarrow \mu^+\mu^-\phi$ candidate. We exclude events where the dimuon invariant mass is within the $J/\psi \rightarrow \mu^+\mu^-$ and $\psi(2S) \rightarrow \mu^+\mu^-$ mass regions to eliminate possible contributions from the charmonium resonant decays.

Muons are required to have $p_T > 1.5$ or 2.0 GeV/c depending on which dimuon trigger selected the event. The kaon requirement is $p_T > 0.4$ GeV/c. The following three discriminating variables are used in the optimization of the searches: the proper lifetime significance, ct/σ_{ct}; the pointing angle α from the B meson candidate to the primary vertex; and the isolation, I, defined as the transverse momentum carried by the B meson candidate divided by the transverse momentum of all charged particles in a cone around the direction of the B meson candidate. The expected number of background events in the B mass window is obtained by extrapolating events in the high-mass sideband to the signal region. Since the region below the B signal window contains partially reconstructed B decays, only the high-mass sideband is used in the background estimate. The figure-of-merit for the optimization is $S/\sqrt{(S+B)}$, where S is the estimate of the expected yield of the rare decays, and B is the expected background. For the B^+ and B^0 rare decay searches, the PDG values of the branching fractions are used in the optimization, while the theoretical expectation is used for the B_s search. The optimization is performed separately for the three rare decay modes. The resulting optimal values are very similar between the different modes and the following averages are used for all three searches: $ct/\sigma_{ct} > 14$, $\alpha < 0.06$, and $I > 0.6$.

The invariant mass distribution for the three searches after applying the optimal requirements on the discriminating variables are shown in Fig. 9. An excess is found in all three modes. The significance of each excess is determined by calculating the probability for the background to fluctuate into the number of observed events or more. A significance of 4.5, 2.9,
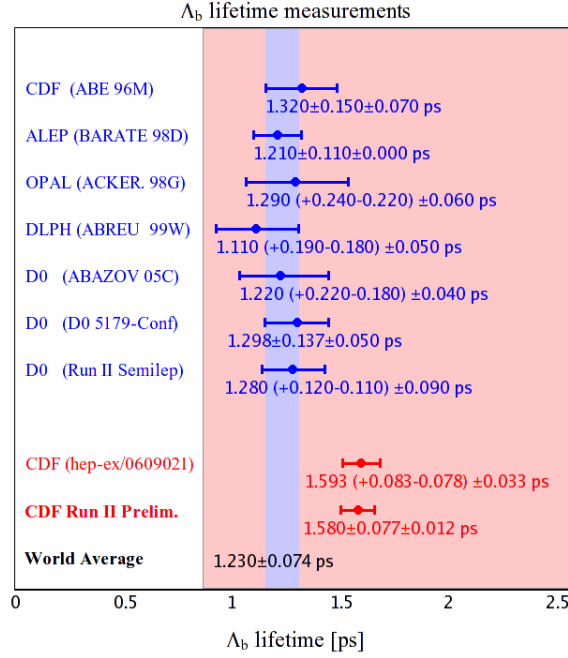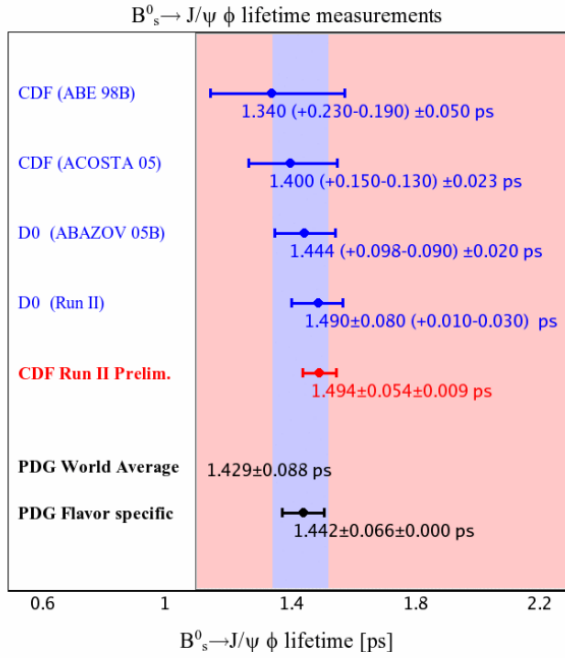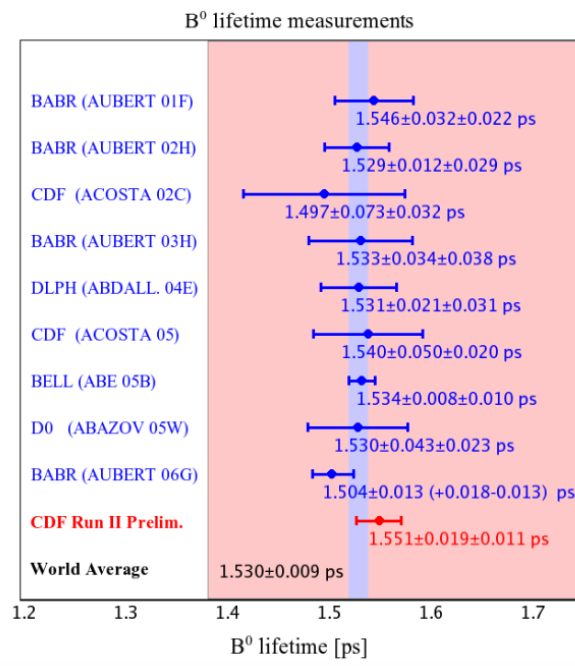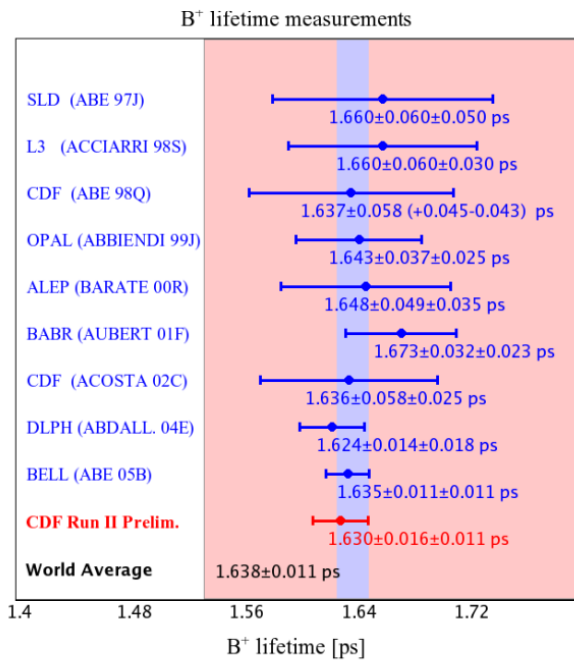
Figure 8: Comparison of measured lifetimes with a selection of results quoted in the PDG2006 and others. Note: the world average values are from PDG2006 and do not include the CDF preliminary results.

and 2.4 standard deviations is found respectively for the B^+, B^0 and B_s modes.

The branching fraction can be computed by normalizing the number of the observed signal to the number of reconstructed resonant $B \to J/\psi h$ decays:

$$\frac{\mathcal{B}(B \to \mu^+\mu^- h)}{\mathcal{B}(B \to J/\psi h)} = \frac{N_{\mu^+\mu^- h}}{N_{J/\psi h}} \frac{\epsilon_{\mu^+\mu^- h}}{\epsilon_{J/\psi h}} \times \mathcal{B}(J/\psi \to \mu^+\mu^-),$$

(6)

where h stands for K^+, K^*, or ϕ. The parameter $N_{\mu^+\mu^- h}$ is either the number of observed signal events or, in the case of setting a limit, the upper limit on the number of signal decays, and $N_{J/\psi h}$ is the number of reconstructed $B \to J/\psi h$ events. The efficiency terms $\epsilon_{\mu^+\mu^- h}$ and $\epsilon_{J/\psi h}$ are the efficiency for reconstructing the normalization and signal decays, respectively.
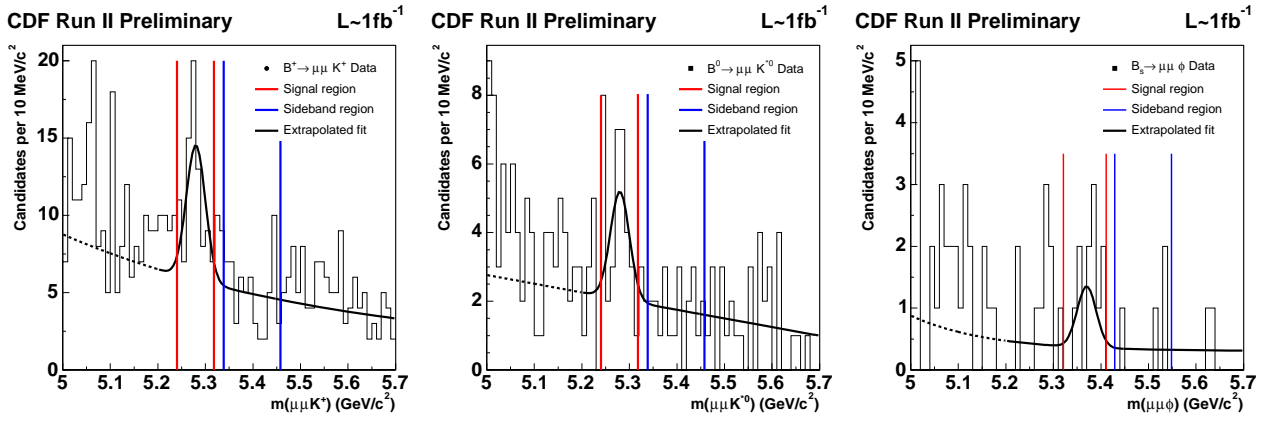
Using the world average branching ratio of the

Figure 9: The invariant distribution for the three rare decay modes. The vertical bars define the signal and sideband regions. The black curve illustrates the expected shape for the signal and combinatoric background.

normalization modes [10], we extract the following branching ratios using Eq. 6:

$$\mathcal{B}(B^+ \to \mu^+\mu^- K^+) = (0.60 \pm 0.15 \pm 0.04) \times 10^{-6},$$
$$\mathcal{B}(B^0 \to \mu^+\mu^- K^{*0}) = (0.82 \pm 0.31 \pm 0.10) \times 10^{-6},$$

first uncertainty is statistical and second systematic. These measurements are consistent with the world average and of similar precision as the best available measurements.

Since the $B_s \to \mu^+\mu^-\phi$ excess is not significant, we calculate a limit on its relative branching ratio using a Bayesian approach. We find:

$$\frac{\mathcal{B}(B_s^0 \to \mu^+\mu^-\phi)}{\mathcal{B}(B_s^0 \to J/\psi\phi)} < 2.30 \times 10^{-3} \text{ at 90\% C.L.} \quad (7)$$

This limit on the B_s mode is the most stringent to date.

6. Charmless Two-Body B Decays: $B^0 \to h^+ h'^-$

The decay modes of B mesons into pairs of charmless pseudoscalar mesons are effective probes of the quark-mixing (CKM) matrix and are sensitive to potential new physics effects. The large production of B hadrons of all kinds at the Tevatron allows an opportunity for measuring such decays in new modes, which are important to supplement our understanding of B meson decays.

6.1. Event Selection and Fit of Composition

B Hadrons are initially selected by using the two-track trigger. In the offline analysis, additional cuts are imposed on isolation, I –defined previously–, and the quality of the fit, χ^2, to the 3D decay vertex of the B hadron candidate. Final selection cuts are determined by an optimization procedure, based on minimizing the expected uncertainty of the physics observables to be measured. Two different sets of cuts are used, optimized respectively for best resolution on $A_{CP}(B^0 \to K^+\pi^-)$ (loose cuts), and for best sensitivity for the discovery of the yet unobserved $B_s^0 \to K^-\pi^+$ mode (tight cuts). The looser set of cuts is also used for measuring the decay rates of the largest yield modes, while the tighter set is used for the other rare modes.

The invariant mass distribution of the candidates, with an arbitrary pion mass assignment to both tracks, shows a single large peak in the B mass range (Fig. 10), formed by several overlapping modes.
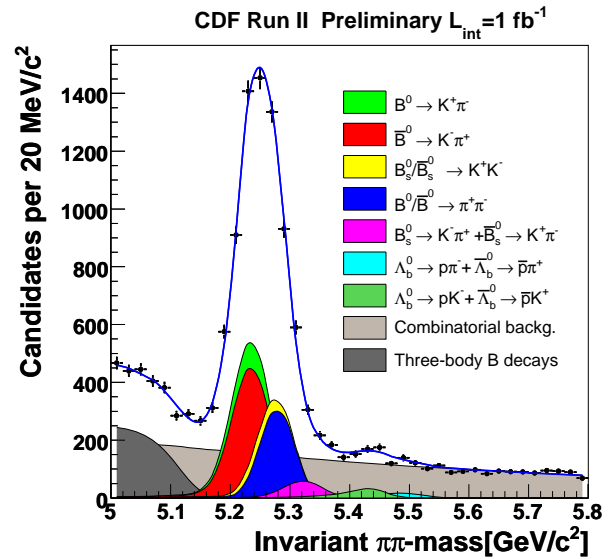

Figure 10: Invariant mass distribution of $B^0 \to h^+ h'^-$ candidates passing the loose selection cuts. The pion mass is assigned to both tracks.

The different modes are statistically separated and individually measured by means of an unbinned maximum-Likelihood fit, combining kinematics and PID. Kinematic information is summarized by three loosely correlated observables: the mass $M_{\pi\pi}$ calculated with the pion mass assignment to both particles; the signed momentum imbalance $\alpha = (1 - p_1/p_2)q_1$, where p_1 (p_2) is the lower (higher) of the particle momenta, and q_1 is the sign of the charge of the particle of momentum p_1; the scalar sum of particle momenta $p_{tot} = p_1 + p_2$. The above variables allow evaluating the mass of the B candidate for any mass assignment to the decay products. PID information is given by a dE/dx measurement for each track.

The shape of the mass distribution of each single channel accounts for non-Gaussian tails, both from resolution and from emission of photons in the final state, which is simulated on the basis of analytical QED calculations [14]. The mass distribution of the combinatorial background is fit to a smooth function, while the physics background is parameterized by an 'Argus function' [15] smeared with our mass resolution. Kinematical distributions for the signal are represented by analytical expressions, while for the combinatorial background are parameterized from the mass sidebands of data.

The dominant contributions to the systematic uncertainty come from: statistical uncertainty on isolation efficiency ratio (for B_s^0 modes); uncertainty on the dE/dx calibration and parameterization; and uncertainty on the combinatorial background model. Smaller systematic uncertainties are assigned for: trigger efficiencies; physics background shape and kinematics; B meson masses and lifetimes.

6.2. Results

The search for rare modes is performed using the tight selection. The fit allows for the presence of any component of the form $B \to h^+ h'^-$ or $\Lambda_b^0 \to ph^-$ where $h, h' = K$ or π, with the yield as a free parameter.

The results provide the first observation of the $B_s^0 \to K^- \pi^+$ mode, with a significance of 8.2σ, which includes systematic uncertainties and is evaluated from Monte Carlo samples of background without signal. The branching fraction of this mode is significantly sensitive to the value of angle γ of the unitary triangle. Our measurement $\mathcal{B}(B_s^0 \to K^- \pi^+) = (5.0 \pm 0.75 \pm 1.0) \times 10^{-6}$ is in agreement with the prediction in [16], but is lower than most other predictions [17–19].

No evidence is found for modes $B_s^0 \to \pi^+ \pi^-$ or $B^0 \to K^+ K^-$, in agreement with expectations of significantly smaller branching fractions. An upper limit for the branching ratio on these decay modes is set:

$$\mathcal{B}(B^0 \to K^+ K^-) \ < 0.7 \times 10^{-6} \quad \text{at 90\% CL,}$$

$$\mathcal{B}(B_s^0 \to \pi^+ \pi^-) \ < 1.36 \times 10^{-6} \quad \text{at 90\% CL.}$$

In the same sample, we also get to observe charmless decays of a B baryon for the first time: $\Lambda_b^0 \to p\pi^-$ (6σ) and $\Lambda_b^0 \to pK^-$ (11.5σ). We measure the ratio of branching fractions of these modes as $\mathcal{B}(\Lambda_b^0 \to p\pi^-)/\mathcal{B}(\Lambda_b^0 \to pK^-) = 0.66 \pm 0.14 \pm 0.08$, in good agreement with the expected range [0.60, 0.62] from [20].

We can measure from our data the asymmetries of both B^0 and B_s^0 decays in the self-tagging final state $K^\pm \pi^\mp$. The asymmetry of the B_s^0 mode is measured with the tight selection, while the looser selection is used for the B^0 mode.

The result $A_{CP}(B^0 \to K^+ \pi^-) = -0.086 \pm 0.023 \pm 0.009$ is in agreement with the world average [21], and is the second most precise measurement.

Using the tight set of cuts CDF is able to achieve the first CP asymmetry measurement on the $B_s^0 \to K^- \pi^+$ system, finding $A_{CP}(B_s^0 \to K^- \pi^+) = 0.39 \pm 0.15 \pm 0.08$. This value favors the large CP asymmetry predicted by the Standard Model and has the correct sign [22], but is still compatible with zero (significance just above 2σ).

7. Conclusions

The heavy flavor physics program at CDF is being very productive. We have reviewed some of the most recent CDF results which make use of ~ 1 fb^{-1}. These results include the observation of the B_s oscillation frequency, the first observation of bottom baryon $\Sigma_b^{(*)\pm}$ states, updates on B hadrons lifetimes, and searches for rare decays in the $b \to s\mu^+\mu^-$ transition and in charmless two-body B decays. CDF achieve complementary and competitive results with B Factories, being some of them unique at CDF. With 2.5 fb^{-1} already on tape we expect more and new interesting results for this summer.

Acknowledgments

The results shown here represent the work of many people. I would like to thank all colleagues from CDF for their efforts to carry out these challenging physics analyses, the conference organizers for a very nice days of physics, and the colleagues of my research institution, IFCA, for all their help.

References

[1] R. Blair *et al.* (CDF Coll.), *"The CDF II detector – Technical Design Report"*, FERMILAB-PUB-96-390-E (1996).

[2] W. Ashmanskas *et al.* (CDF Coll.), *"The CDF Silicon Vertex Trigger"*, Nucl. Instrum. Meth. **A518**:532 (2004), [physics/0306169].

[3] S. Eidelman *et al.*, Phys. Lett. **B592**, 1.

[4] V. M. Abazov *et al.* (D0 Coll.), *"Direct Limits on the B_s Oscillation Frequency"*, Phys. Rev. Lett. **97** (2006) 021802.

[5] A. Abulencia *et al.* (CDF Coll.), *"Measurement of the $B_s^0 - \overline{B}_s^0$ Oscillation Frequency"*, Phys. Rev. Lett. **97** (2006) 062003.

[6] A. Abulencia *et al.* (CDF Coll.), *"Observation of $B_s^0 - \overline{B}_s^0$ Oscillations"*, Phys. Rev. Lett. **97** (2006) 242003.

[7] T. Sjörstrand *et al.*, Computer Phys. Commun. **135**, 238 (2001).

[8] H. G. Moser and A. Roussarie, Nucl. Instrum. Methods Phys. Res., Sect. A **384**, 491 (1997).

[9] I. I. Y. Bigi, M. A. Schifman and N. Uraltsev, Ann. Rev.Nucl. Part. Sci. **47** 591 (1997).

[10] W.-M. Yao *et al.*, Journal of Physics **G 33**, 1 (2006).

[11] B. Aubert *et al.* (BABAR Coll.), Phys. Rev. D **73**, 092001 (2006).

[12] A. Ishikawa *et al.* (Belle Coll.), Phys. Rev. Lett. **91**, 261601 (2003).

[13] C. Q. Geng and C. C. Liu, J. Phys. G **29**, 1103 (2003).

[14] E. Baracchini and G. Isidori, Phys. Lett. B **633**, 309 (2006).

[15] H. Albretch *et al.*, Phys. Lett. B **241**, 278 (1990).

[16] A. R. Williamson and J. Zupan, Phys. Rev. D **74**, 014003 (2006).

[17] M. Beneke and M. Neubert, Nucl. Phys. B **675**, 333 (2003).

[18] X. Q. Yu, Y. Li and C. D. Lu, Phys. Rev. D **71**, 074026 (2005).

[19] J. F. Sun, G. H. Zhu, and D. S. Du, Phys. Rev. D **68**, 054003 (2003).

[20] R. Mohanta *et al.*, Phys. Rev. D **63**, 074001 (2001).

[21] E. Barberio *et al.* [Heavy Flavor Averaging Group (HFAG)], arXiv:hep-ex/0603003.

[22] M. Gronau, Phys. Lett. B **492**, 297 (2000).